Numerical Solution for a Non-Fickian Diffusion in a Periodic Potential

Adérito Araújo[1], Amal K. Das[2], Cidália Neves[1,3] and Ercília Sousa[1,*]

[1] *CMUC, Department of Mathematics, University of Coimbra, 3001-454 Coimbra, Portugal.*
[2] *Department of Physics, Dalhousie University, Halifax, Nova Scotia B3H 3J5, Canada.*
[3] *ISCAC, Polytechnic Institute of Coimbra, 3040-316 Coimbra, Portugal.*

Abstract. Numerical solutions of a non-Fickian diffusion equation belonging to a hyperbolic type are presented in one space dimension. The Brownian particle modelled by this diffusion equation is subjected to a symmetric periodic potential whose spatial shape can be varied by a single parameter. We consider a numerical method which consists of applying Laplace transform in time; we then obtain an elliptic diffusion equation which is discretized using a finite difference method. We analyze some aspects of the convergence of the method. Numerical results for particle density, flux and mean-square-displacement (covering both inertial and diffusive regimes) are presented.

AMS subject classifications: 35L15, 60K40, 60J65, 65R10, 65M06, 65M12
PACS: 02.60.Lj, 05.40.Jc
Key words: Numerical methods, Laplace transform, telegraph equation, periodic potential, non-Fickian diffusion.

1 Introduction

In this paper we shall present numerical solutions of a non-Fickian diffusion equation in the presence of a symmetric periodic potential in one space dimension. Let us briefly recall that the familiar Fickian diffusion equation for a particle density $n(\xi,\tau)$, in the presence of a potential $V(\xi)$ reads

$$\frac{\partial n}{\partial \tau}(\xi,\tau) = D\frac{\partial^2 n}{\partial \xi^2}(\xi,\tau) + \frac{1}{m\gamma}\frac{\partial}{\partial \xi}\left[\frac{dV}{d\xi}(\xi) n(\xi,\tau)\right], \tag{1.1}$$

*Corresponding author. *Email addresses:* alma@mat.uc.pt (A. Araújo), akdas@dal.ca (A. K. Das), cneves@iscac.pt (C. Neves), ecs@mat.uc.pt (E. Sousa)

where ξ is the space variable, τ is time, γ is a friction parameter and $D = k_B T/m\gamma$ is the diffusion coefficient, m being the mass of the Brownian particle whose overdamped (diffusive) dynamics is well described by (1.1); k_B is the Boltzmann's constant and T the temperature of the fluid.

The equation of our study is

$$\frac{1}{\gamma}\frac{\partial^2 n}{\partial \tau^2}(\xi,\tau)+\frac{\partial n}{\partial \tau}(\xi,\tau)=D\frac{\partial^2 n}{\partial \xi^2}(\xi,\tau)+\frac{1}{m\gamma}\frac{\partial}{\partial \xi}\left[\frac{dV}{d\xi}(\xi)n(\xi,\tau)\right]. \tag{1.2}$$

Both equations, (1.1) and (1.2) can be derived from an underlying kinetic equation, e.g. the phase-space Kramers equation [9]

$$\frac{\partial f}{\partial \tau}+\frac{p}{m}\frac{\partial f}{\partial \xi}-\frac{dV}{d\xi}\frac{\partial f}{\partial p}=\gamma\frac{\partial}{\partial p}(pf)+mk_BT\gamma\frac{\partial^2 f}{\partial p^2}, \tag{1.3}$$

where $f(\xi,p,\tau)$ is the probability density function for the position component ξ and momentum component p of the Brownian particle.

Eq. (1.2) in the absence of a potential field is sometimes referred to as the telegrapher equation although we shall call it a non-Fickian diffusion equation. We refer to [9] for a derivation of (1.2) from (1.3). It may be noted that for times larger than $1/\gamma$, the first term on the left hand side of (1.2) can be neglected and the Fickian regime is regained. Eq. (1.1) in the absence of a potential field leads to the well known result for the mean square displacement [11]

$$<\xi^2(\tau)>=2D\tau. \tag{1.4}$$

In the presence of a flexible symmetric potential, it was shown in [9] that $<\xi^2(\tau)>$ does not necessarily behave linearly with time. Eq. (1.2) retains some short time inertial behaviour of a Brownian particle and at long time results in a diffusive behaviour. The velocity $v = d\xi/d\tau$ of a Brownian particle is not well defined in the diffusive regime for which (1.1) is applicable. Since (1.2) is applicable in an inertial regime, the velocity can be calculated with (1.2). Quite recently the instantaneous velocity of a Brownian particle has been experimentally investigated [12, 13, 18]. This provides an additional motivation for studying (1.2). There is also a recent paper [5] which models transport of ions in insulating media through a non-Fickian diffusion equation of the type discussed in our work. In [5] the non-Fickian diffusion equation is referred to as a hyperbolic diffusion equation.

To solve our problem we consider a numerical method based on a finite difference discretization and time Laplace transform. The latter is suitable for long times and also for solutions that are not necessarily smooth in time. It may be noted that iterative methods in time, including implicit methods such as the Crank-Nicolson [8], which allow a choice of large time steps, usually take too long to compute the solution.

The paper is organized as follows. In Section 2 we present the model problem in dimensionless variables. In Section 3 we describe a numerical method based on the time Laplace transform which is suitable for long time integration and also for solutions which

are not very smooth. In Section 4 the convergence properties of the algorithm are studied. In Section 5 we present the behaviour of the solution to the non-Fickian diffusion equation, the flux and the mean square displacement. We conclude the paper, in Section 6, with a summary and outlook.

2 The model and physical quantities

In our studies we consider three quantities of physical interest. These are the particle density $n(\xi,\tau)$, the current density (flux) $j(\xi,\tau)$ and the mean square displacement $<\xi^2(\tau)>$. The current density is not normally studied. However, since we are dealing with a non-Fickian diffusion equation we have decided to consider $j(\xi,\tau)$ as well. For the Fickian case and in the absence of any potential, $j(\xi,\tau)$ is related to $n(\xi,\tau)$ through $j=-D(\partial n/\partial\xi)$. This is not so in the non-Fickian case for which the relation between $j(\xi,\tau)$ and $n(\xi,\tau)$ is more involved.

Let us consider the non-Fickian diffusion equations for particle density and the flux

$$\frac{1}{\gamma}\frac{\partial^2 n}{\partial\tau^2}+\frac{\partial n}{\partial\tau}=-\frac{1}{m\gamma}\frac{\partial}{\partial\xi}(Pn)+D\frac{\partial^2 n}{\partial\xi^2}, \tag{2.1}$$

$$j+\frac{1}{\gamma}\frac{\partial j}{\partial\tau}=-D\frac{\partial n}{\partial\xi}-\frac{1}{m\gamma}Pn, \tag{2.2}$$

with $n(\xi,\tau)$ as the density of the Brownian particles. P is the force acting on the particle due to the potential field V, i.e.,

$$P=-\frac{dV}{d\xi}.$$

We consider a symmetric periodic potential field, as previously studied in [6], [9] and [14]. It reads

$$V(\xi;\alpha)=\frac{1}{J_0(\mathbf{i}\alpha)}e^{\alpha\cos\xi}-1, \tag{2.3}$$

where J_0 is the Bessel function of the first kind and zero order and $\mathbf{i}$ is the imaginary unit. In order to illustrate the flexible form of this single-parameter potential we have plotted, Fig. 1, the potential (2.3), for two values of the parameter, $\alpha=1$ and $\alpha=16$.

Our model consists of Eqs. (2.1) and (2.2), and the potential field $V(\xi;\alpha)$ given by (2.3). For later purpose we introduce the following dimensionless parameters

$$n=\frac{n}{n_0},\qquad x=\frac{\xi}{\sqrt{D/\gamma}},\qquad t=\tau\gamma, \tag{2.4}$$

where n_0 is a reference particle density (concentration). The dimensionless forms of (1.2)

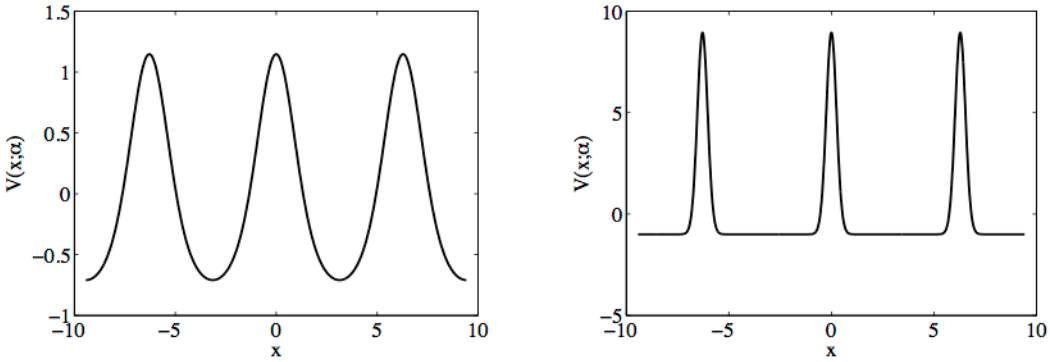

Figure 1: Potential field $V(x;\alpha)$. Left: $\alpha=1$; Right: $\alpha=16$.

and (2.2) can be written as

$$\frac{\partial^2 n}{\partial t^2}+\frac{\partial n}{\partial t}=-\frac{\partial}{\partial x}(Pn)+\frac{\partial^2 n}{\partial x^2}, \tag{2.5}$$

$$j+\frac{\partial j}{\partial t}=-\sqrt{D}\sqrt{\gamma}\frac{\partial n}{\partial x}+\gamma P(x)n, \tag{2.6}$$

with

$$P(x)=-\frac{1}{m\sqrt{D\gamma^3}}\frac{dV}{dx}. \tag{2.7}$$

3 Numerical method

We consider equations (2.5) and (2.6) with the following initial conditions

$$n(x,0)=\frac{1}{L\sqrt{\pi}}e^{-x^2/L^2}, \qquad \frac{\partial n}{\partial t}(x,0)=0, \tag{3.1}$$

$$j(x,0)=\frac{1}{L\sqrt{\pi}}e^{-x^2/L^2}\left(\frac{\sqrt{D}\sqrt{\gamma}}{L^2}2x+\gamma P(x)\right), \tag{3.2}$$

where

$$P(x)=-\frac{1}{m\sqrt{D\gamma^3}}\frac{dV}{dx}, \qquad V(x;\alpha)=\frac{1}{J_0(\mathrm{i}\alpha)}e^{\alpha\cos x}-1.$$

The boundary conditions are given by

$$\lim_{x\to\infty} n(x,t)=0, \qquad \lim_{x\to-\infty} n(x,t)=0, \tag{3.3}$$

$$\lim_{x\to\infty} j(x,t)=0, \qquad \lim_{x\to-\infty} j(x,t)=0. \tag{3.4}$$

In this section we describe a numerical method to solve the problem (2.5)-(2.6). Our approach can be pursued in three steps. First, we apply the Laplace transform to (2.5)-(2.6) in order to remove the time dependent terms and we obtain an ordinary differential equation in x that also depends on the Laplace transform parameter s. Secondly, we solve the ordinary differential equation thus obtained, by using a finite difference scheme. Lastly, using a numerical inverse Laplace transform algorithm we obtain the final approximate solution.

3.1 Spatial discretization

Our numerical method is facilitated if we apply time Laplace transform to Eq. (2.5) and obtain the ordinary differential equation

$$\frac{d^2\widetilde{n}}{dx^2}-\lambda_s\widetilde{n}-\frac{d}{dx}(P\widetilde{n})=-(1+s)n(x,0), \tag{3.5}$$

where $\lambda_s=s^2+s$; s is a complex variable and $\widetilde{n}$ is the Laplace transform of n defined by

$$\widetilde{n}(x,s)=\int_0^\infty \mathrm{e}^{-st}n(x,t)dt. \tag{3.6}$$

Now, assume we have a space discretization $x_i=a+i\Delta x$, $i=0,\cdots,N$. Let $\widetilde{\eta}_i(s)$, $i=0,\cdots,N$ represent the approximation of $\widetilde{n}(x_i,s)$ in the Laplace transform domain. The outflow boundary is such that $\widetilde{\eta}_N(s)=0$, for all s and N sufficiently large, which is according to the physical boundary condition.

To derive the numerical method we consider central differences to approximate the first derivative and the second derivative of Eq. (3.5). We obtain, for a fixed s, the finite difference scheme given by

$$\frac{\widetilde{\eta}_{i-1}(s)-2\widetilde{\eta}_i(s)+\widetilde{\eta}_{i+1}(s)}{\Delta x^2}-\lambda_s\widetilde{\eta}_i(s)-\frac{P_{i+1}\widetilde{\eta}_{i+1}(s)-P_{i-1}\widetilde{\eta}_{i-1}(s)}{2\Delta x}=-(1+s)n(x_i,0), \tag{3.7}$$

for $i=1,\cdots,N-1$, where $P_i=P(x_i)$.

Therefore, we obtain the linear system

$$K(s)\widetilde{\mathfrak{J}}(s)=\widetilde{b}(s), \tag{3.8}$$

where $K(s)=[K_{i,j}(s)]$ is a band matrix of size $N-1\times N-1$ with bandwidth three and $\widetilde{\mathfrak{J}}(s)=[\widetilde{\eta}_1(s),\cdots,\widetilde{\eta}_{N-1}(s)]^T$. The matrix $K(s)$ has entries of the form

$$K_{i,i-1}(s)=\frac{1}{\Delta x^2}+\frac{P_{i-1}}{2\Delta x}, \tag{3.9a}$$

$$K_{i,i}(s)=-\frac{2}{\Delta x^2}-\lambda_s, \tag{3.9b}$$

$$K_{i,i+1}(s)=\frac{1}{\Delta x^2}-\frac{P_{i+1}}{2\Delta x}, \tag{3.9c}$$

and $\widetilde{b}(s)$ contains boundary conditions being represented by

$$\widetilde{b}(s)=\begin{bmatrix} -(1+s)n(x_1,0) \\ -(1+s)n(x_2,0) \\ \vdots \\ -(1+s)n(x_{N-2},0) \\ -(1+s)n(x_{N-1},0) \end{bmatrix}+\begin{bmatrix} -K_{1,0}(s)\widetilde{\eta}_0(s) \\ 0 \\ \vdots \\ 0 \\ -K_{N-1,N}(s)\widetilde{\eta}_N(s) \end{bmatrix}. \tag{3.10}$$

To compute the flux, we apply the Laplace transform to Eq. (2.6), that is,

$$(1+s)\widetilde{j}=-\sqrt{D}\sqrt{\gamma}\frac{d\widetilde{n}}{dx}+\gamma P(x)\widetilde{n}+j(x,0), \tag{3.11}$$

where $\widetilde{j}$ is the Laplace transform of the flux j. The last step is to determine an approximate solution $\eta_i(t)$ and $j_i(t)$ of $n(x_i,t)$ and $j(x_i,t)$ respectively, which is obtained from $\widetilde{\eta}_i(s)$ and $\widetilde{j}_i(s)$ by using a Laplace inversion numerical method.

3.2 Laplace transform inversion

In this section, we determine an approximate solution $\eta_i(t)$ from $\widetilde{\eta}_i(s)$ by using a Laplace inversion numerical method. For the sake of clarity we omit the index i, denoting $\widetilde{\eta}_i(s)$ by $\widetilde{\eta}(s)$.

A formally exact inverse Laplace transform of $\widetilde{\eta}(s)$ into $\overline{\eta}(t)$ is given through the Bromwich integral [15]

$$\overline{\eta}(t)=\frac{1}{2\pi\mathbf{i}}\int_{\beta-\mathbf{i}\infty}^{\beta+\mathbf{i}\infty}\mathrm{e}^{st}\widetilde{\eta}(s)\,ds, \tag{3.12}$$

where β is such that the contour of integration is to the right-hand side of any singularity of $\widetilde{\eta}(s)$. However, for a numerical evaluation the above integral is first transformed to an equivalent form

$$\overline{\eta}(t)=\frac{1}{\pi}\mathrm{e}^{\beta t}\int_0^{\infty}\mathrm{Re}\left\{\widetilde{\eta}(s)\mathrm{e}^{\mathbf{i}\omega t}\right\}d\omega, \tag{3.13}$$

where $s=\beta+\mathbf{i}\omega$ [1, 15, 16]. The integral is now evaluated through the trapezoidal rule [1,7], with step size π/T, and we obtain

$$\overline{\eta}(t)=\frac{1}{T}\mathrm{e}^{\beta t}\left[\frac{\widetilde{\eta}(\beta)}{2}+\sum_{k=1}^{\infty}\mathrm{Re}\left\{\widetilde{\eta}\left(\beta+\frac{\mathbf{i}k\pi}{T}\right)\mathrm{e}^{\frac{\mathbf{i}k\pi t}{T}}\right\}\right]-E_T, \tag{3.14}$$

for $0<t<2T$ and where E_T is the discretization error. It is known that the infinite series in this equation converges very slowly. To accelerate the convergence, we apply the quotient-difference algorithm, proposed in [2], and also used in [16], to calculate the series in (3.14) by the rational approximation in the form of a continued fraction. Under some conditions we can always associate a continued fraction to a given power series.

We denote $v(z)$ the continued fraction

$$v(z)=d_0/(1+d_1z/(1+d_2z/(1+\cdots))) \tag{3.15}$$

associated with the power series in (3.14). For $z=e^{i\pi t/T}$,

$$v(z)=\frac{\widetilde{\eta}(\beta)}{2}+\sum_{k=1}^{\infty}\widetilde{\eta}\left(\beta+\frac{ik\pi}{T}\right)z^k, \tag{3.16}$$

and the coefficients d_p's of (3.15) are obtained by recurrence relations from the coefficients $\widetilde{\eta}(\beta+\frac{ik\pi}{T})$, that is, denoting $\widetilde{\eta}_k$ the coefficients $\widetilde{\eta}(\alpha+\frac{ik\pi}{T})$, let

$$e_0^{(k)}=0, \qquad q_1^{(k)}=\widetilde{\eta}_{k+1}/\widetilde{\eta}_k, \qquad k=0,1,\cdots. \tag{3.17}$$

From the recurrence relations,

$$e_p^{(k)}+q_p^{(k)}=e_{p-1}^{(k+1)}+q_p^{(k+1)}, \qquad k=0,1,\cdots, \quad p=1,2,\cdots, \tag{3.18}$$

$$q_{p+1}^{(k)}e_p^{(k)}=q_p^{(k+1)}e_p^{(k+1)}, \qquad k=0,1,\cdots, \quad p=1,2,\cdots, \tag{3.19}$$

we obtain the coefficients d_p's,

$$d_0=\widetilde{\eta}_0, \qquad d_{2p-1}=-q_p^{(0)}, \qquad d_{2p}=-e_p^{(0)}, \qquad p=1,2,\cdots. \tag{3.20}$$

Let the M-th partial fraction be denoted by $v(z,M)$. Therefore

$$v(z)=v(z,M)+E_F^M,$$

where E_F^M is the truncation error. Then

$$\overline{\eta}(t)=\frac{1}{T}e^{\beta t}\mathrm{Re}\left\{v(z,M)+E_F^M\right\}-E_T.$$

The approximation for $\overline{\eta}(t)$ is denoted by $\eta(t)$ and given by

$$\eta(t)=\frac{1}{T}e^{\beta t}\mathrm{Re}\{v(z,M)\}.$$

4 Convergence of the numerical method

In this section we discuss the convergence of the numerical method chosen to compute an approximate solution to Eq. (2.5). Let us denote by $\widetilde{E}_S$ the error associated with the spatial discretization, that is,

$$\widetilde{n}(x_i,s)=\widetilde{\eta}_i(s)+\widetilde{E}_S(x_i,s). \tag{4.1}$$

The next errors come from the numerical inversion of Laplace transform, where the Laplace inverse transform of $\widetilde{\eta}_i(s)$ is, as described in the previous section, the solution

$$\overline{\eta}_i(t)=\frac{1}{T}e^{\beta t}\mathrm{Re}\left\{v(z,M_i)+E_F^M(x_i,t)\right\}-E_T(x_i,t), \tag{4.2}$$

where E_T is the error associated with the trapezoidal approximation and E_F^M is the truncation error associated with the continued fraction. Note that for each x_i the algorithm chooses a M_i and therefore for each x_i we have a different value of the approximation of the continued fraction, $v(z,M_i)$. Therefore from (4.1)-(4.2) we have

$$n(x_i,t)=\frac{1}{T}e^{\beta t}\mathrm{Re}\left\{v(z,M_i)+E_F^M(x_i,t)\right\}-E_T(x_i,t)+E_S(x_i,t),$$

where $E_S(x_i,t)$ is the inverse Laplace transform of the error $\widetilde{E}_S(x_i,s)$.

4.1 Approximation errors E_T and E_F

The error E_T that comes from the integral approximation using the trapezoidal rule, according to Crump [7], is

$$E_T=\sum_{n=1}^{\infty}e^{-2n\beta T}n(x_i,2nT+t).$$

Assume now that our function is bounded such as $|n(x_i,t)|\leq e^{\sigma t}$, for all x_i. Note that, in this case the Laplace transform $\widetilde{n}(s)$, Eq. (3.6), is defined for $\mathrm{Re}(s)>\sigma$ and therefore β on (3.12) must be $\beta>\sigma$. Therefore the error can be bounded by

$$E_T\leq e^{\sigma t}\sum_{n=1}^{\infty}e^{-2nT(\beta-\sigma)}=\frac{e^{\sigma t}}{e^{2T(\beta-\sigma)}-1},\qquad 0<t<2T.$$

It follows that by choosing β sufficiently larger than σ, we can make E_T as small as desired. For practical purposes and in order to choose a convenient β we use the inequality which bounds the error

$$E_T\leq e^{\sigma t-2T(\beta-\sigma)}.$$

If we want to have the bound $E_T\leq b_T$ then by applying the logarithm in both sides of the previous inequality we have

$$\beta\geq\sigma\frac{2T+t}{2T}-\frac{1}{2T}\ln(b_T).$$

Assuming $\sigma\geq 0$ we can write

$$\beta\geq\sigma-\frac{\ln(b_T)}{2T}.$$

In our example we consider $\sigma=0$. In practice the trapezoidal error E_T is controlled by the parameter β we choose.

The second error, E_F^M, comes from the approximation of the continued fraction given by (3.16). This error is controlled by imposing a tolerance TOL such as

$$|v(z,M)-v(z,M-1)|<TOL,$$

in order to get the approximation $\eta_i(t)$ given by

$$\eta_i(t)=\frac{1}{T}e^{\beta t}\mathrm{Re}\{v(z,M_i)\}, \tag{4.3}$$

where M_i changes according to which x_i we are considering.

In order to understand better how to control the trapezoidal error with the parameter β and how the tolerance TOL affects the error, we present a test example which is an analytically exactly solvable model. We assume P constant and Fickian diffusion

$$\frac{\partial n}{\partial t}=-P\frac{\partial n}{\partial x}+D\frac{\partial^2 n}{\partial x^2}, \qquad x\in]0,\infty[, \quad t>0. \tag{4.4}$$

The initial condition is

$$n(x,0)=0 \tag{4.5}$$

and the boundary conditions are

$$n(0,t)=N_0, \qquad n(\infty,t)=0. \tag{4.6}$$

It will be noted that we are now considering a semi-infinite geometry. We note the difference between this test case and our original unbound problem. We choose this test example for two reasons: Firstly, Eq. (4.4) can be analytically exactly solved by first applying the time-Laplace transform and then through the inverse Laplace transform. Secondly, this example is chosen to compare the convergence aspects of the Laplace inversion algorithm without spatial discretization.

If we apply the Laplace transform to this problem we obtain

$$\widetilde{n}(x,s)=N_0\frac{1}{s}e^{P/2D-x\sqrt{(P/2D)^2+s}}. \tag{4.7}$$

The analytical solution is given by

$$n(x,t)=\frac{N_0}{2}\left(\mathrm{erfc}\left[\frac{x-Pt}{2\sqrt{Dt}}\right]+e^{Px/D}\mathrm{erfc}\left[\frac{x+Pt}{2\sqrt{Dt}}\right]\right). \tag{4.8}$$

In Figs. 2 and 3, for $N_0=1$, $P=2$, $t=1$ and $0\leq x\leq 12$, we plot the following errors,

$$E_F=\max_{1\leq i\leq N-1}|v(z,M_i)-v(z,M_i-1)|, \tag{4.9}$$

$$E_G=\max_{1\leq i\leq N-1}|n(x_i,t)-\eta_i(t)|. \tag{4.10}$$

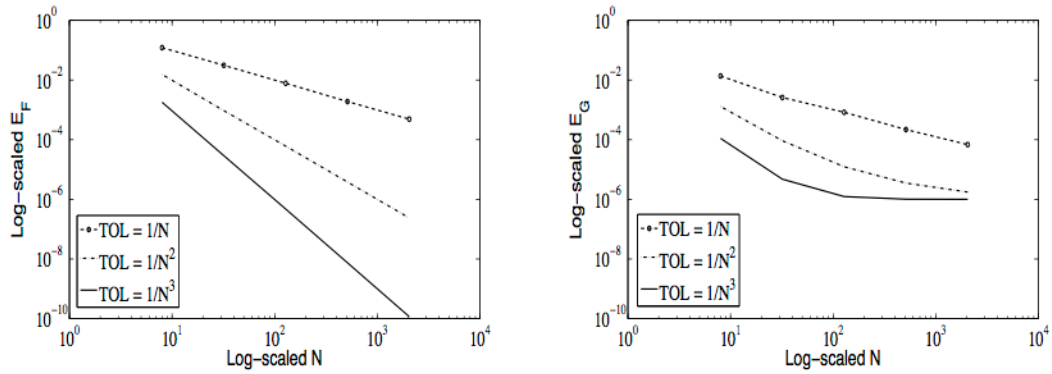

Figure 2: Error E_F and E_G for $N_0=1$, $P=2$, $t=1$, $0\leq x\leq 12$ and $\beta=-\ln(10^{-6})/2T$ with $T=20$ and different values of TOL. The global error is controlled by the parameter β.

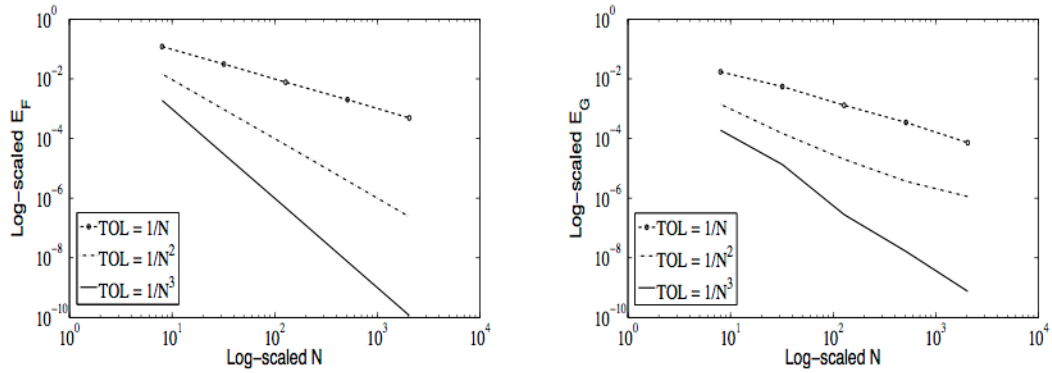

Figure 3: Error E_F and E_G for $N_0=1$, $P=2$, $t=1$, $0\leq x\leq 12$ and $\beta=-\ln(10^{-10})/2T$ with $T=20$ and different values of TOL. The parameter β is chosen such that the global error is not affected.

We choose the interval $0\leq x\leq 12$ in order to avoid the influence of the right numerical boundary condition in the numerical computations, that in this case is $n(12,t)=0$.

The error E_F is related with the error E_F^M since we control E_F^M by controlling E_F with the tolerance TOL. Figs. 2 and 3 show how the parameter β, given by $\beta=-\ln(10^{-6})/2T$ in Fig. 2 and $\beta=-\ln(10^{-10})/2T$ in Fig. 3, affects the global convergence. Note that in Fig. 2 the precision does not go further than 10^{-6}. The global error of Figs. 2 and 3 is not affected by the spatial error E_S since we apply the Laplace inversion algorithm directly in (4.7).

The Laplace inversion algorithm approximates the value of the infinite series using a truncated continued fraction and this truncation is done by choosing an M_i for each x_i. This M_i is chosen according to which value of the tolerance TOL we consider. To show an example with a region involving a very steep gradient, let us consider the problem which consists of Eq. (2.5), for $P=2$, with initial conditions $n(x,0)=0$ and $\frac{\partial n}{\partial t}(x,0)=0$ and boundary conditions $n(0,t)=1$ and $n(\infty,t)=0$. We show in Fig. 4 the variations of M_i

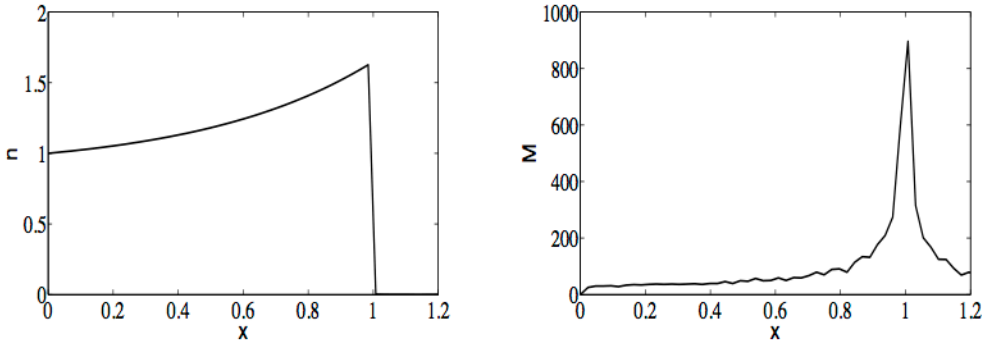

Figure 4: Number of iterations M for $P=2$, $t=1$, $TOL=1/N^2$, and $\beta=-\ln(10^{-10})/2T$ with $T=20$. Left: Approximate solution; Right: Number of iterations for each x_i.

and it is clear the algorithm concentrates the high values of M in the region that presents steep gradients.

4.2 Spatial discretization error $\widetilde{E}_S(x_i,s)$

We now turn to the discretization error $\widetilde{E}_S(x_i,s)$, defined in (4.1) (our main problem), and prove that it is of second order. Let us denote the differential operator L given by

$$L\widetilde{n}=\frac{d^2\widetilde{n}}{dx^2}-\lambda_s\widetilde{n}-\frac{d}{dx}(P\widetilde{n}).$$

We also denote by L_π the operator associated with the spatial discretization, given by

$$L_\pi\widetilde{n}(x_i,s)=\frac{\widetilde{n}_{i-1}(s)-2\widetilde{n}_i(s)+\widetilde{n}_{i+1}(s)}{\Delta x^2}-\lambda_s\widetilde{n}_i(s)-\frac{P_{i+1}\widetilde{n}_{i+1}(s)-P_{i-1}\widetilde{n}_{i-1}(s)}{2\Delta x},$$

where $\widetilde{n}_i(s)$ denotes the exact solution at $\widetilde{n}(x_i,s)$. The local truncation error is given by

$$T_e(x_i,s)=L_\pi\widetilde{n}(x_i,s)-L\widetilde{n}(x_i,s).$$

For a fixed s, we make a Taylor expansions of the functions $\widetilde{n}$ and P around the point x_i. We obtain, for a sufficiently smooth $\widetilde{n}$,

$$\begin{aligned}
&K_{i,i-1}(s)\widetilde{n}_{i-1}(s)+K_{i,i}(s)\widetilde{n}_i(s)+K_{i,i+1}(s)\widetilde{n}_{i+1}(s)+(1+s)n(x_i,0)\\
=&\frac{d^2\widetilde{n}_i}{dx^2}(s)-\lambda_s\widetilde{n}_i(s)-\frac{d}{dx}(P\widetilde{n})_i(s)+(1+s)n(x_i,0)\\
&+\left[-\frac{1}{6}P_i'''\widetilde{n}_i(s)-\frac{1}{2}P_i''\frac{d\widetilde{n}_i}{dx}(s)-\frac{1}{2}P_i'\frac{d^2\widetilde{n}_i}{dx^2}(s)-\frac{1}{6}P_i\frac{d^3\widetilde{n}_i}{dx^3}(s)+\frac{1}{12}\frac{d^4\widetilde{n}_i}{dx^4}(s)\right]\Delta x^2\\
&+\mathcal{O}(\Delta x^3),
\end{aligned}$$

where P', P'', P''' denotes the derivatives of P (unlike in the previous test example P is now not a constant). From this result we can conclude that, for $\widetilde{n}(.,s) \in C^4(\mathbb{R})$, we have

$$||T_e||_\infty = \max_{2\leq i\leq N} |T_e(x_i,s)| \leq c\Delta x^2.$$

By denoting $\widetilde{E}_i = \widetilde{E}_S(x_i,s)$, $i=1,\cdots,N-1$ we have

$$L_\pi \widetilde{E}_i = T_e(x_i,s),$$

that is,

$$K(s)\widetilde{E}(s) = T_e(s).$$

If $||K^{-1}(s)||_\infty \leq C$ then $|\widetilde{E}_i| \leq C||T_e||_\infty$. Since the matrix $K(s)$ is not an M-matrix [19,20], it is not easy to prove analytically the inverse of $K(s)$ is bounded. This difficulty is related to the set of values of the parameter λ_s, given by

$$\lambda_s = s^2+s = \beta^2+\beta-\omega^2+\mathrm{i}\omega(2\beta+1), \qquad \omega = \frac{k\pi}{T}, \quad k=1,\cdots,M,$$

where M defines the set of values in the Laplace domain, since for $\omega^2 > \beta^2+\beta$ the complex λ_s has negative real part. However, it is easy to see numerically that for a fixed T, where T defines the stepsize of the trapezoidal rule used to approximate the integral (3.13), as we refine the space step, the value $||K^{-1}(s)||_\infty$ does not change significantly. We also observe that $||K^{-1}(s)||_\infty$ is larger for values of $|s|$ close to zero, indicating that the convergence can be slower for these values, as can be observed in Fig. 5.

Additionally we observe that we have a similar phenomenon to the so-called pollution effect [3] observed for the Helmholtz equation and high wavenumbers where the discretization space step has to be sufficiently refined to avoid numerical dispersion. Also in this context it is observed that if we have a complex number as a coefficient in the equation, which is our case with λ_s, the imaginary part acts as an absorption parameter, which seems to allow us to better control the solution by decreasing the solution magnitude [10]. Following what is reported in literature [3,4,17], a useful rule observed for an adjustment of the space step is to force some relation between T and the Δx. For our problem a similar condition is

$$\omega\Delta x \leq \frac{2\pi}{10}. \tag{4.11}$$

This leads to $(M/T)\Delta x \leq 2/10$, with $M = \max_i M_i$, where M_i is the iteration for each x_i, as given in (4.3).

We have discussed the consistency and stability of the numerical method. Regarding the accuracy of the numerical method, additionally to the truncation errors, let us look at the condition number of the matrix $K(s)$, $\mathrm{cond}(K)$, that determines how accurately we can solve the system (3.8). The condition number of the matrix $K(s)$ is affected by the values of T and N as we can observe in Figs. 6 and 7. We can infer from these figures that the

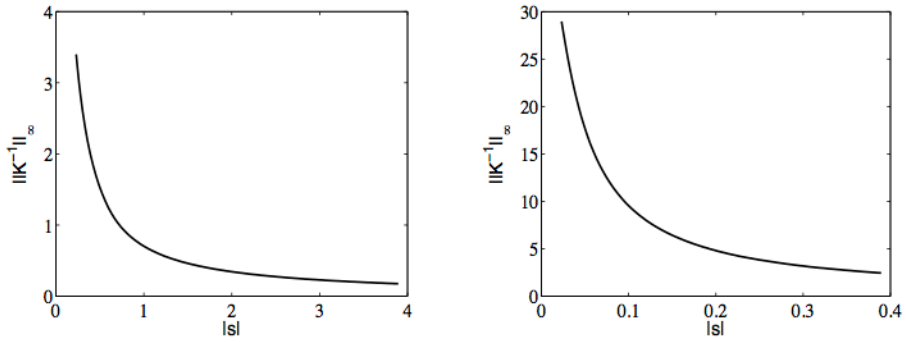

Figure 5: Infinity norm of the matrix $K^{-1}(s)$ for $N=1000$. We have considered $P(x)$ with $\alpha=1$. Left: $T=80$; Right: $T=800$.

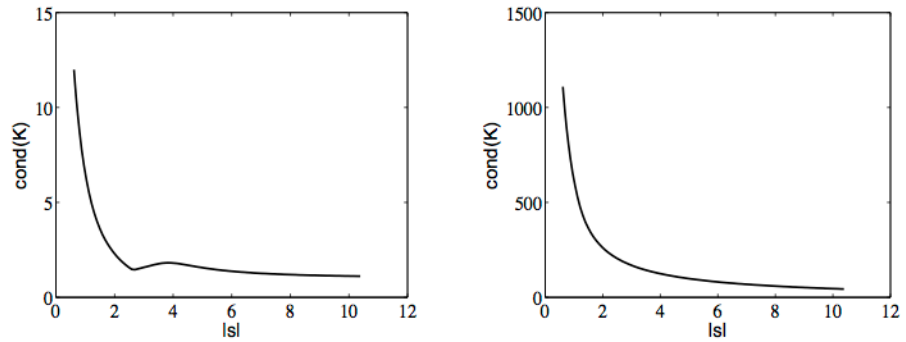

Figure 6: Condition number for the matrix $K(s)$ for $T=30$. We have considered $P(x)$ with $\alpha=1$. Left: $N=50$; Right: $N=500$.

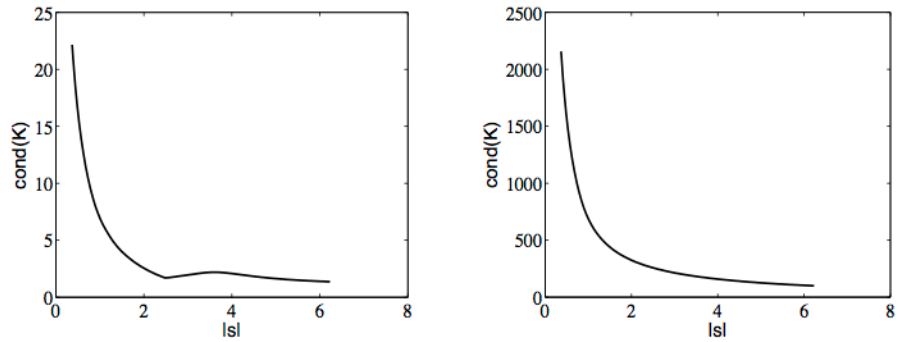

Figure 7: Condition number for the matrix $K(s)$ for $T=50$. We have considered $P(x)$ with $\alpha=1$. Left: $N=50$; Right: $N=500$.

condition number of the matrix K increases if we increase T or N. Usually one must always expect to loose $\log_{10}(\text{cond}(K))$ digits of precision in computing the solution, except under very special circumstances. Since we are working with double precision numbers,

about 16 decimal digits of accuracy, caution is advised when the condition number is much greater than $1/\sqrt{10^{-16}}$, which in general does not happen for our problem. The condition number of order 10^6 is reached for very large values of T and N, such as, both larger than 10^5. We plotted the results for $\alpha=1$, although for different values of α we have similar results.

4.3 Numerical tests

In order to illustrate the full feature of the numerical method, we consider two test problems. We will show that the order of convergence of the numerical method is second order as predicted by the theoretical analysis. Additionally we will compare the computational efficiency with classical methods, such as, the Crank-Nicolson (CN).

The computational cost of the Laplace algorithm [2] for inverting the function $\tilde{\eta}_i(s)$ is $\mathcal{O}(M_i^2)$ and therefore the total cost for the Laplace transform inversion is $\mathcal{O}\left(\sum_{i=1}^{N} M_i^2\right)$. The computational cost for solving the linear system of equations resulting from the finite difference discretization is approximately $\mathcal{O}\left(\overline{M}N\right)$, where we define $\overline{M}$ as the average of $\{M_i, i=1,\cdots,N\}$. Therefore, the total cost of the numerical method that uses inverse Laplace transforms and a finite difference discretization (Laplace FD) is approximately

$$\mathcal{O}\left(\sum_{i=1}^{N} M_i^2 + \overline{M}N\right) \approx \mathcal{O}\left((\overline{M}^2 + \overline{M})N\right).$$

Since we expect $\mathcal{O}(\overline{M})$ to be much smaller than $\mathcal{O}(N)$, we also expect the computational cost of Laplace FD method to be much less than the computational cost of numerical methods like Crank-Nicolson (CN) where the computational cost is $\mathcal{O}\left(N^2\right)$. We will see this indeed happens in the two examples we present bellow, which consist of a Fickian and a non-Fickian problem.

In order to measure the gain in efficiency, we consider the variable Gain given by

$$\text{Gain} = \frac{\#\text{ operations CN} - \#\text{ operations Laplace FD}}{\max\{\#\text{ operations CN}, \#\text{ operations Laplace FD}\}}.$$

First, we consider the Fickian problem (4.4)-(4.6), whose exact solution is given by (4.8). In Table 1 and Fig. 8 we show the global error (4.10), for $N_0=1$, $P=2$, $t=1$ and different values of the space step. We also present, for the Laplace FD method, the parameter T chosen, the number of iterations $M=\max_i M_i$, the average of the M_i's, denoted by $\overline{M}$ and the rate of convergence. We observe that the Laplace FD method is more efficient than the CN method. The advantage of the Laplace FD method in the computational cost increases with N, that is, as Δx decreases.

In Table 2 and Fig. 9 we increase the time to $t=20$ and for the CN method we consider the same timestep Δt we have considered previously for the results obtained in Table 1. As expected, the efficiency of Laplace FD method is more evident as shown by the values of the variable Gain. We also note that the computational cost of the inverse Laplace

Table 1: Fickian case: Global error (4.10) for $P=2$, $t=1$, $0\le x\le 10$, $TOL=1/N^3$, $\beta=-\ln(10^{-16})/2T$, $\Delta t=\Delta x/10$.

Δx	CN	Laplace FD	Rate	T	M	$\overline{M}$	Gain
10/128	0.2567×10^{-3}	0.2549×10^{-3}		3	14	9	29.7%
10/256	0.6427×10^{-4}	0.6601×10^{-4}	2.0	3	16	11	48.4%
10/512	0.1608×10^{-4}	0.1615×10^{-4}	2.0	3	18	13	64.5%
10/1024	0.4019×10^{-5}	0.4063×10^{-5}	2.0	3	20	15	76.5%
10/2048	0.1001×10^{-5}	0.1018×10^{-5}	2.0	3	21	17	85.1%

Table 2: Fickian case: Global error (4.10) for $P=2$, $t=20$, $0\le x\le 70$, $TOL=1/N^3$, $\beta=-\ln(10^{-16})/2T$, $\Delta t=\Delta x/70$.

Δx	CN	Laplace FD	Rate	T	M	$\overline{M}$	Gain
70/128	0.3116×10^{-2}	0.3210×10^{-2}		30	12	8	97.2%
70/256	0.7788×10^{-3}	0.8620×10^{-3}	1.9	30	13	10	97.9%
70/512	0.1949×10^{-3}	0.1886×10^{-3}	2.2	30	14	12	98.5%
70/1024	0.4651×10^{-4}	0.4675×10^{-4}	2.0	30	16	13	99.1%
70/2048	0.1218×10^{-4}	0.1229×10^{-4}	1.9	30	16	15	99.4%

Table 3: Fickian case: Global error (4.10) for $P=2$, $t=20$, $0\le x\le 70$, $TOL=1/N^3$, $\beta=-\ln(10^{-16})/2T$, $\Delta t=20\Delta x/70$.

Δx	CN	Laplace FD	Rate	T	M	$\overline{M}$	Gain
70/128	0.3589×10^{-2}	0.3210×10^{-2}		30	12	8	43.8%
70/256	0.8991×10^{-3}	0.8620×10^{-3}	1.9	30	13	10	57.0%
70/512	0.2249×10^{-3}	0.1886×10^{-3}	2.2	30	14	12	69.5%
70/1024	0.5622×10^{-4}	0.4675×10^{-4}	2.0	30	16	13	82.2%
70/2048	0.1506×10^{-4}	0.1229×10^{-4}	1.9	30	16	15	88.3%

transform algorithm is reduced. This can be easily seen by looking at the values of M and $\overline{M}$ in Tables 1 and 2. In Table 3, we also consider $t=20$ but we increase the timestep Δt. The Laplace FD method is now slightly more accurate and is still with less computational effort than the CN method.

Now, we turn to the non-Fickian problem given by the telegraph equation,

$$\frac{\partial n}{\partial t}+\frac{\partial^2 n}{\partial t^2}=D\frac{\partial^2 n}{\partial x^2},\qquad x\in]0,2\pi[,\quad t>0, \tag{4.12}$$

with initial conditions

$$n(x,0)=\sin(\frac{x}{2}),\qquad \frac{\partial n}{\partial t}(x,0)=-\frac{1}{2}\sin(\frac{x}{2}), \tag{4.13}$$

and boundary conditions

$$n(0,t)=0,\qquad n(2\pi,t)=0. \tag{4.14}$$

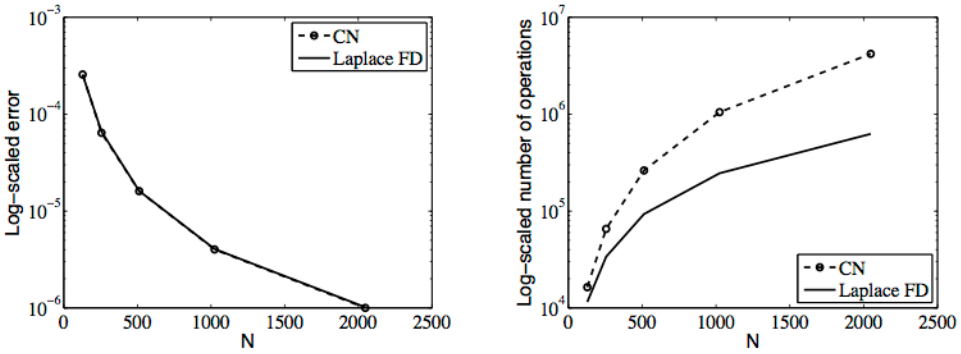

Figure 8: Fickian case (Table 1). Left: Global error; Right: Total cost.

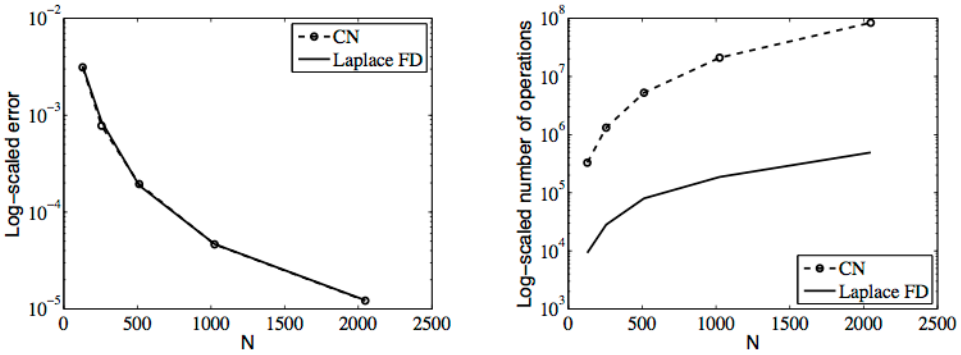

Figure 9: Fickian case (Table 2). Left: Global error; Right: Total cost.

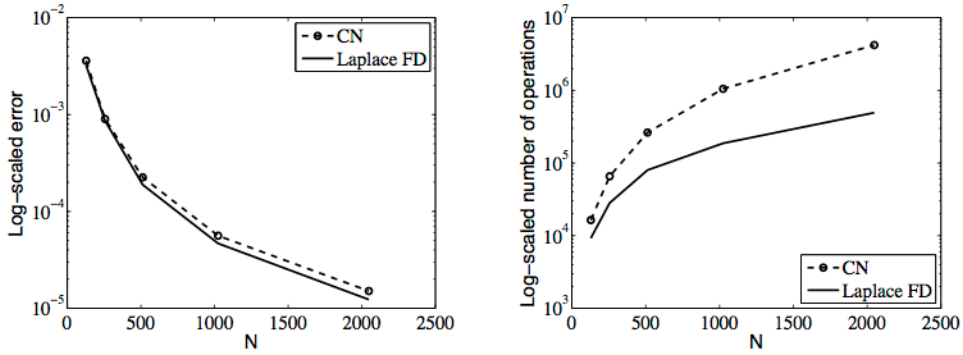

Figure 10: Fickian case (Table 3). Left: Global error; Right: Total cost.

We can easily obtain the analytical solution given by

$$n(x,t) = e^{-\frac{t}{2}} \sin(\frac{x}{2}). \tag{4.15}$$

As for the Fickian case, we present in Table 4 and Fig. 11, the global error (4.10) for $t = 1$

Table 4: Non-Fickian case: Global error (4.10) for $t=1$, $0\le x\le 2\pi$, $TOL=1/N^3$, $\beta=-\ln(10^{-16})/2T$, $\Delta t=\Delta x/(2\pi)$.

Δx	CN	Laplace FD	Rate	T	M	$\overline{M}$	Gain
$2\pi/128$	0.3420×10^{-5}	0.4864×10^{-5}		5	19	18	-66.3%
$2\pi/256$	0.8551×10^{-6}	0.7019×10^{-6}	2.8	4	19	18	-25.2%
$2\pi/512$	0.2138×10^{-6}	0.2893×10^{-6}	1.3	4	21	20	18.0%
$2\pi/1024$	0.5357×10^{-7}	0.6196×10^{-7}	2.2	3	20	19	62.9%
$2\pi/2048$	0.1339×10^{-7}	0.1509×10^{-7}	2.0	3	24	21	77.4%

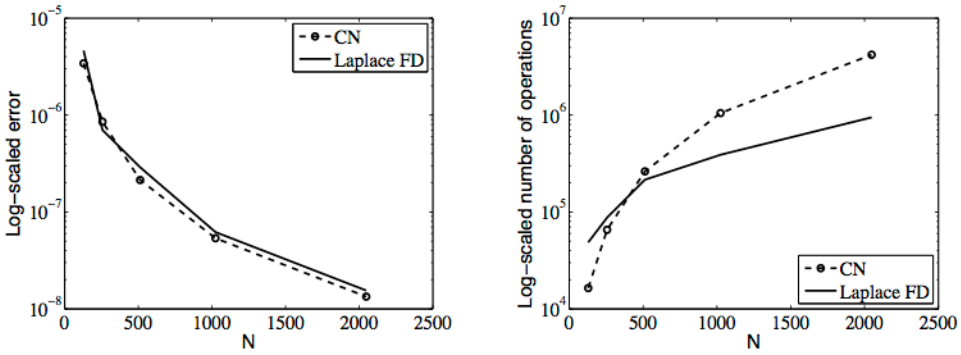

Figure 11: Non-Fickian case (Table 4). Left: Global error; Right: Total cost.

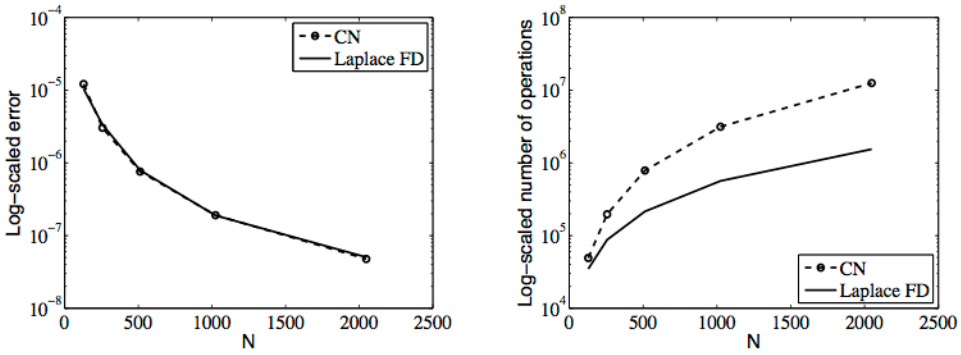

Figure 12: Non-Fickian case (Table 5). Left: Global error; Right: Total cost.

and different space steps. The solution of this problem is smoother than the solution of the previous problem which has an initial discontinuity in the corner $(x,t)=(0,0)$. In this case the CN method behaves better than previously. However, the Laplace FD method is still more efficient, specially if we look for higher order accuracy. Furthermore, we observe in Table 5 and Fig. 12 that if we increase the time to $t=3$, the superiority of the Laplace FD method is also more evident.

It will be noted that our main problem is unbounded. But with at least one zero

Table 5: Non-Fickian case: Global error (4.10) for $t=3$, $0\le x\le 2\pi$, $TOL=1/N^3$, $\beta=-\ln(10^{-16})/2T$, $\Delta t=\Delta x/(2\pi)$.

Δx	CN	Laplace FD	Rate	T	M	$\overline{M}$	Gain
$2\pi/128$	0.1218×10^{-4}	0.1044×10^{-4}		10	16	15	29.2%
$2\pi/256$	0.3044×10^{-5}	0.3368×10^{-5}	1.6	10	18	17	55.5%
$2\pi/512$	0.7610×10^{-6}	0.7942×10^{-6}	2.1	10	20	19	72.7%
$2\pi/1024$	0.1907×10^{-6}	0.1895×10^{-6}	2.1	10	23	22	82.0%
$2\pi/2048$	0.4767×10^{-7}	0.5053×10^{-7}	1.9	10	27	26	87.7%

boundary condition for each, the two test examples (Fickian and non-Fickian), although semi-bounded and bounded respectively, can be computationally viewed as similar to our main problem. We observe from the previous results that we obtain second order convergence as predicted by the theoretical analysis for the main problem.

5 Numerical results for $n(x,t)$, $j(x,t)$ and $<x^2(t)>$

To do the numerical experiments we consider the equations

$$\frac{\partial^2 n}{\partial t^2}+\frac{\partial n}{\partial t}=-\frac{\partial}{\partial x}(Pn)+\frac{\partial^2 n}{\partial x^2}, \tag{5.1}$$

$$j+\frac{\partial j}{\partial t}=-\frac{\partial n}{\partial x}+Pn, \tag{5.2}$$

for

$$P(x)=-\frac{dV}{dx} \qquad \text{and} \qquad V(x;\alpha)=\frac{1}{J_0(\mathbf{i}\alpha)}e^{\alpha\cos x}-1.$$

For $\alpha=1$, the potential is smoother compared with $\alpha=16$, as it is shown in Fig. 13. In Fig. 13 we observe that $P(x)$ for $\alpha=1$ changes between -1 and 1, whereas for $\alpha=16$ changes between -20 and 20 and the change is not smooth. Our method can deal very well with both cases.

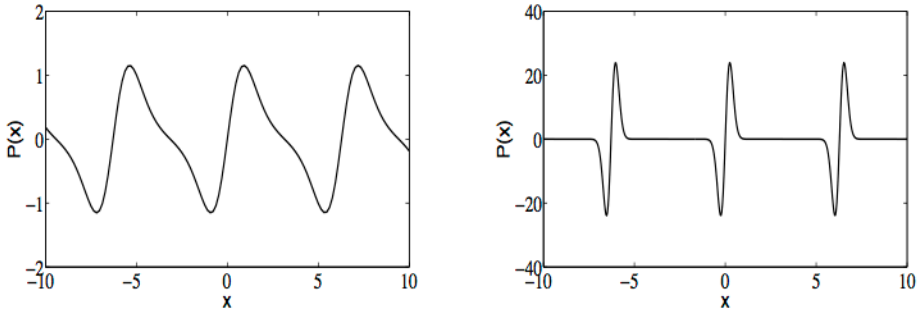

Figure 13: Potential $P(x)$. Left: $\alpha=1$; Right: $\alpha=16$.

We consider the initial conditions,

$$n(x,0) = \frac{1}{L\sqrt{\pi}}e^{-x^2/L^2}, \quad \frac{\partial n}{\partial t}(x,0)=0, \tag{5.3}$$

$$j(x,0) = \frac{1}{L\sqrt{\pi}}e^{-x^2/L^2}\left(\frac{1}{L^2}2x+P(x)\right), \tag{5.4}$$

and the boundary conditions are given by

$$\lim_{x\to\infty} n(x,t)=0 \quad \text{and} \quad \lim_{x\to-\infty} n(x,t)=0.$$

Note that the stationary solution of the problem is given by

$$n_{st}(x)=N_r\exp(-V(x)),$$

where N_r is a normalization value.

For $\alpha=1$ we show in Figs. 14 and 15 the behaviour of the solution as we increase time from $t=1$ until $t=500$. The peak starts to split into two and then we have several

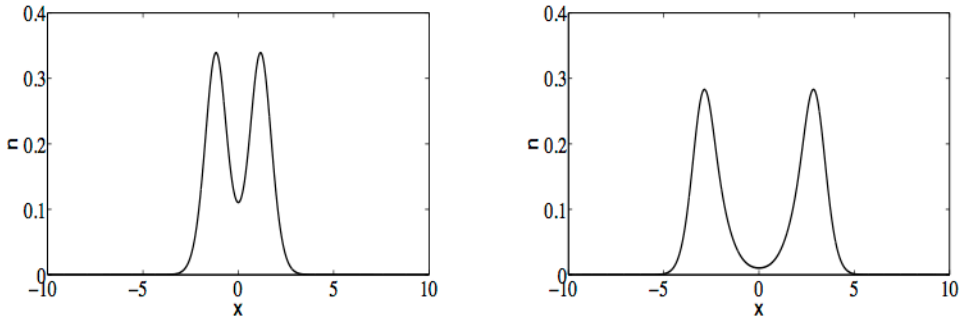

Figure 14: Particle density $n(x,t)$ for $\alpha=1$. Left: Curve for instant of time $t=1$; Right: Curve for instant of time $t=3$.

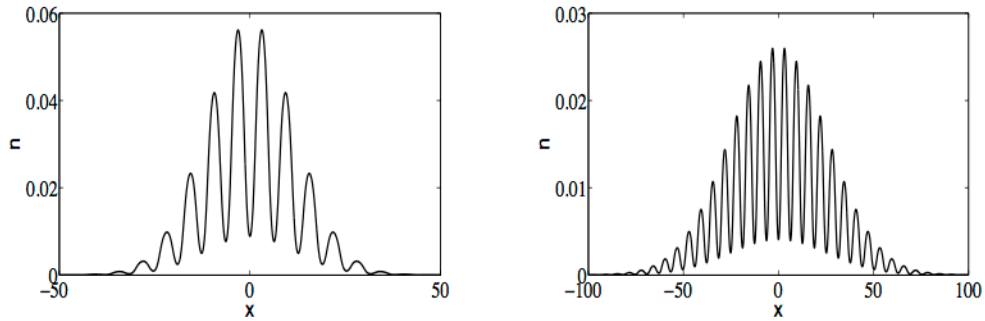

Figure 15: Particle density $n(x,t)$ for $\alpha=1$. Left: Curve for instant of time $t=100$; Right: Curve for instant of time $t=500$.

waves forming that goes to the right and left. The domain where the function is not zero becomes larger as we travel in time. For that reason the computational domain increases considerably which requires more computational effort regarding the discretization in space. For an iterative method where we need to consider a discretization in time, it would require more computational effort for long times as we need to iterate in time whereas the Laplace transform has the advantage of not iterating in time and therefore it is the same if we compute the solution for short times or long times.

In Fig. 16 we plot the flux for $\alpha=1$, as it evolves from $t=0$ to $t=1$ and in Fig. 17 as it evolves from $t=5$ to $t=30$.

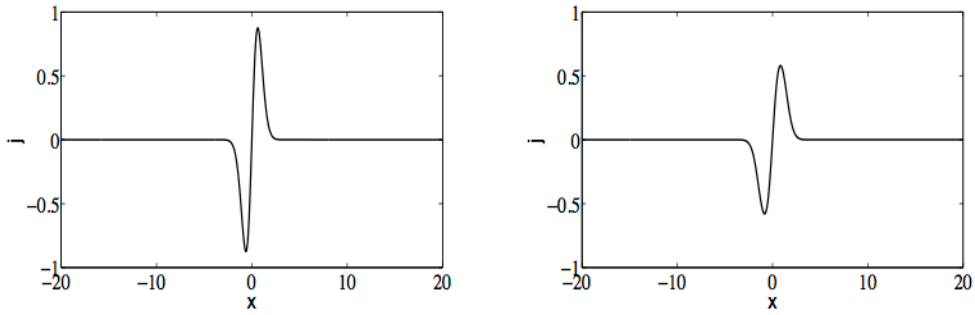

Figure 16: Density flux $j(x,t)$ for $\alpha=1$. Left: Curve for instant of time $t=0$; Right: Curve for instant of time $t=1$.

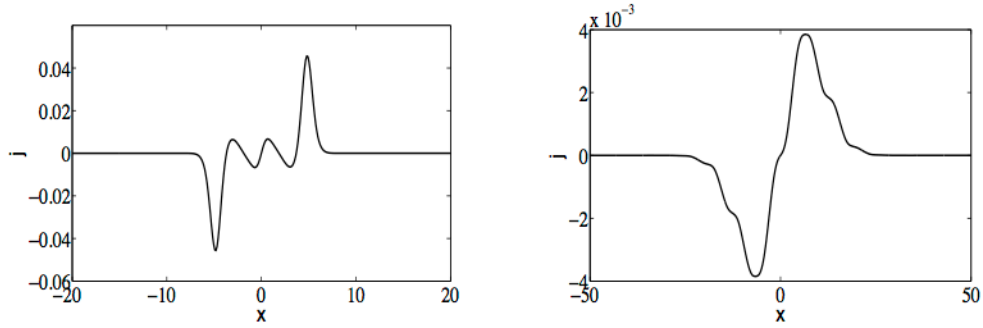

Figure 17: Density flux $j(x,t)$ for $\alpha=1$. Left: Curve for instant of time $t=5$; Right: Curve for instant of time $t=30$.

A quantity of physical interest in diffusion problems is the mean square displacement defined by

$$<x^2(t)>=\int_{-\infty}^{\infty}[x^2n(x,t)]dx.$$

For the Fickian case, $<x^2(t)>$ is linear in t for all times in the absence of a potential. Now we would like to present calculations of $<x^2(t)>$ for the non-Fickian diffusion. At short times, and in the presence of a potential, the mean square displacement, $<x^2(t)>$,

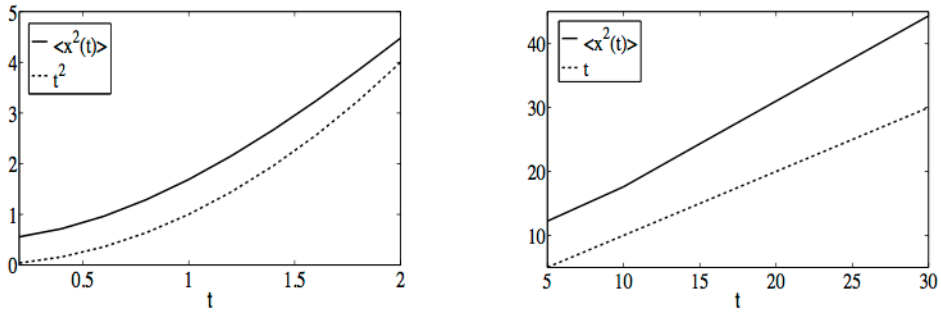

Figure 18: Mean square displacement for $\alpha=1$; Left: Curves for $t\in[0,2]$; Right: Curves for $t\in[5,30]$.

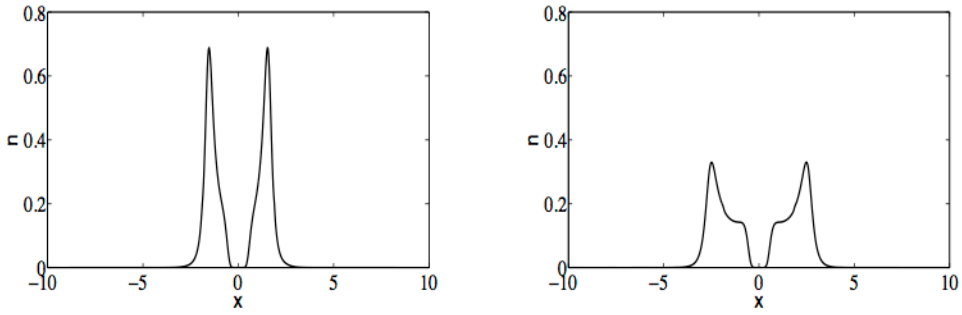

Figure 19: Particle density $n(x,t)$ for $\alpha=16$. Left: Curve for instant of time $t=1$; Right: Curve for instant of time $t=2$.

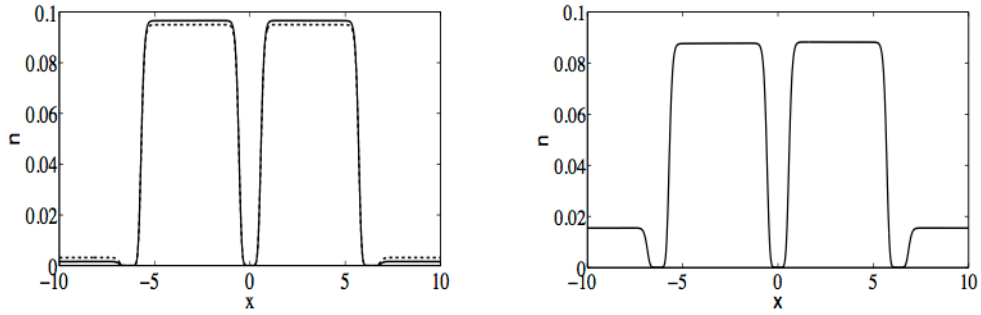

Figure 20: Particle density $n(x,t)$ for $\alpha=16$. Left: Curves for instant of times $t=500$ $(-)$, $t=1000$ $(--)$; Right: Curve for instant of time $t=5000$ $(-)$.

shows a t^2 behaviour, see Fig. 18. This is due to inertial effects which are captured by a non-Fickian diffusion equation.

For $\alpha=16$ we show the evolution of the solution in the first instants of time. We see the solution presents very steep gradients and the method is able to give accurate solutions. First we observe how the wave split for $t=1$ and $t=2$ in Fig. 19.

Next in Fig. 20 we observe the behaviour for very large times. It is interesting to see

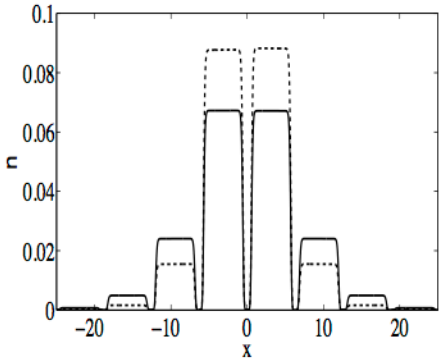

Figure 21: Particle density $n(x,t)$ for $\alpha=16$. Curves for instant of time $t=5000$ $(--)$; $t=10000$ $(-)$.

how the Laplace method is able to give very quickly solutions for very large times. An iterative numerical method in time, it would take a large amount of time to run experiments for such long times such as $t=5000$ or $t=10000$ as we can see in Fig. 21. The flux for $\alpha=16$ is plotted in Fig. 22.

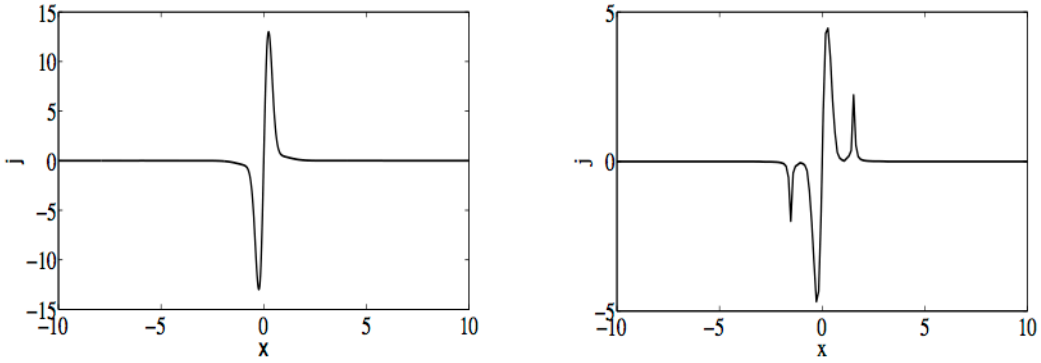

Figure 22: Density flux for $\alpha=16$. Left: Curve for instant of time $t=0$; Right: Curve for instant of time $t=1$.

6 Summary and outlook

In this paper we have presented a numerical solution of a non-Fickian diffusion equation which is a partial differential equation of the hyperbolic type. This equation is of physical interest in the context of Brownian motion in inertial as well as diffusive regimes. In our model the Brownian particle is subjected to a symmetric periodic potential of flexible shapes (generated with a single variable parameter) which can lead to harmonic, anharmonic or a confining potential for the particle.

Instead of introducing discretization in both space and time variables we dealt with the time-derivatives through time Laplace transform and obtained an ordinary differen-

tial equation in space variable. This equation was then solved with a finite-difference scheme, leading to a discretized approximate solution for $\widetilde{n}(x,s)$; the solution is approximate due to discretization and is still formally exact in the Laplace domain s. The next step consisted of numerical Laplace inversion to obtain an approximation to the original solution $n(x,t)$. We show that the full method is second order accurate; this finding receives additional support from two test examples considered in Section 4. One may be able to consider further improvement. A major advantage of using the time Laplace transform is that we can compute the approximate solution for long times accurately and quickly. Any iterative numerical method would take too long to compute the solution for similar times even if we consider an unconditionally implicit numerical method which will allow large time steps. Additionally, our algorithm takes into consideration the smoothness of the solution; in other words the computational effort is higher in the regions where the solution has steep gradients. Another merit of the method is that it can be easily generalized to higher spatial dimensions. It would be of interest to consider an application of the method to numerically solve the Kramers equation which is a more involved partial differential equation than the non-Fickian diffusion equation.

Acknowledgments

We acknowledge the referees for their helpful comments. Research partially supported by the research project UTAustin/MAT/066/2008.

References

[1] J. Abate, W. Whitt, Numerical inversion of Laplace transforms of probability distributions, ORSA Journal on Computing, 7(1) (1995), 36–43.
[2] J. Ahn, S. Kang, Y. Kwon, A flexible inverse Laplace transform algorithm and its application, Computing 71(2) (2003), 115–131.
[3] I.M. Babuska, S.A. Sauter, Is the pollution effect of the FEM avoidable for the Helmholtz equation considering high wave numbers?, SIAM Review 42(3) (2000), 451–484.
[4] G. Bao, G.W. Wei, S. Zhao, Numerical solution of the Helmholtz equation with high wavenumbers, International Journal for Numerical Methods in Engineering 59 (2004), 389–408.
[5] G. Barbero, J. R. Macdonald, Transport process of ions in insulating media in the hyperbolic diffusion regime, Phys. Rev. E 81(5) (2010), 051503.
[6] A.C. Branka, A.K. Das, D.M. Heyes, Overdamped Brownian motion in periodic symmetric potentials, J.Chem.Phys. 113(22) (2000), 9911–9919.
[7] K. Crump, Numerical inversion of Laplace transforms using a Fourier series approximation, Journal of the Association for Computing Machinery 23(1) (1976), 89–96.
[8] J. Crank, P. Nicolson, A practical method for numerical evaluation of solutions of partial differential equations of the heat conduction type, Proc. Cambridge Phil. Soc. 43 (1947), 50–67.
[9] A.K. Das, A non-Fickian diffusion equation, J.Appl.Phys. 70(3) (1991), 1355–1358.

[10] G. Fibich, B. Ilan, S. Tsynkov, Backscattering and nonparaxiality arrest collapse of damped nonlinear waves, SIAM J. Appl. Math. 63(5) (2003), 1718–1736.
[11] J. Fort, V. Méndez, Wavefronts in time-delayed reaction-diffusion systems. Theory and comparison to experiment, Rep. Prog. Phys. 65 (2002), 895–954.
[12] R. Huang et al, Direct observation of the full transition from ballistic to diffusive Brownian motion in a liquid, Nature Physics, NPHYS1953, 2011.
[13] T. Li, S. Kheifets, D. Medellin, M. G. Raizen, Measurement of the instantaneous velocity of a Brownian particle, Science 25(328) (2010), 1673–1675.
[14] M.O. Magnasco, Forced thermal ratchets, Physical Review Letters 71 (1993), 1477–1481.
[15] J.E. Marsden, M.J. Hoffman, Basic Complex Analysis, W.H. Freeman, 1999.
[16] C. Neves, A. Araújo, E. Sousa, Numerical approximation of a transport equation with a time-dependent dispersion flux, in AIP Conference Proceedings 1048 (2008), 403–406.
[17] F.S.B.F. Oliveira, K. Anastasiou, An efficient computational model for water wave propagation in coastal regions, Applied Ocean Research, 20(5) (1998), 263–271.
[18] P.N. Pusey, Brownian motion goes ballistic, Science 332 (2011), 802–803.
[19] K. Wang, C. You, A note on identifying generalized diagonally dominant matrices, International Journal of Computer Mathematics 84(12) (2007), 1863–1870.
[20] R.S. Varga, Matrix Iterative Analysis, Springer, 2000.